CrossMark

J. Plasma Phys. (2015), *vol.* 81, 905810602 © Cambridge University Press 2015
doi:10.1017/S0022377815001087

Linear and nonlinear behaviour of two-stream instabilities in collisionless plasmas

Y. W. Hou[1,†], M. X. Chen[2], M. Y. Yu[3,4] and B. Wu[5]

[1]Key Laboratory of Neutronics and Radiation Safety, Institute of Nuclear Energy Safety Technology, Chinese Academy of Science, Hefei, Anhui 230031, China

[2]School of Electronic Science and Applied Physics, Hefei University of Technology, Hefei, Anhui 230009, China

[3]Institute for Fusion Theory and Simulation and Department of Physics, Zhejiang University, Hangzhou 310027, China

[4]Institute for Theoretical Physics I, Ruhr University, D-44780 Bochum, Germany

[5]Institute of Plasma Physics, Chinese Academy of Sciences, Hefei, Anhui 230031, China

(Received 5 August 2015; revised 30 August 2015; accepted 3 September 2015)

The transient, growth and nonlinear saturation stages in the evolution of the electrostatic two-stream instabilities as described by the Vlasov–Poisson system are reconsidered by numerically following the evolution of the total wave energy of the plasma oscillations excited from (numerical) noise. Except for peculiarities related to the necessarily finite (even though very small) magnitude of the perturbations in the numerical simulation, the existence and initial growth properties of the instabilities from the numerical results are found to be consistent with those from linear normal mode analysis and the Penrose criteria. However, contradictory to the traditional point of view, the growth of instability before saturation is not always linear. The initial stage of the growth can exhibit fine structures that can be attributed to the harmonics of the excited plasma oscillations, whose wavelengths are determined by the system size and the numerical noise. As expected, saturation of the unstable oscillations is due to electron trapping when they reach sufficiently large amplitudes.

1. Introduction

Beam instabilities in collisionless plasmas have been extensively investigated experimentally (Deneef, Malmberg & O'Neil 1973; Van-Wakeren & Hopman 1975; Whelan & Stenzel 1983; Hartmann *et al.* 1995), analytically (Penrose 1960; Clemmow & Dougherty 1969; Infeld & Skorupski 1970; Schamel 1982; Chen 1984; El-Labany & Rowlands 1986; Rostomian 1994; Boyd & Sanderson 2003; Ng, Bhattacharjee & Skiff 2004), and numerically (Roberts & Berk 1967; Morse & Nielson 1969; Gentle & Hohr 1973; Lacina, Krlin & Korbel 1976; Morey & Boswell 1989; Fijalkow & Nocera 2005; Dieckmann *et al.* 2006; Zheng *et al.* 2006; Daldorff *et al.* 2011; Volokitin & Krafft 2012). The linear problem is usually considered analytically by solving the corresponding normal mode eigenvalue problems and unstable modes with different phase velocities but similar growth rates have been found. In this paper, we

† Email address for correspondence: yawei.hou@fds.org.cn

https://doi.org/10.1017/S0022377815001087 Published online by Cambridge University Press

numerically solve the Vlasov–Poisson system and follow the evolution of the total wave energy of an initially bi-Maxwellian electron distribution. It is found that the evolution of the instabilities initiated by numerical noise have three distinct stages: a short transient stage; the growth stage that can involve different modes/harmonics at different growth rates; and the nonlinear saturation stage corresponding to electron trapping in the enhanced wave field.

2. Simulation model

The one-dimensional Vlasov–Poisson system is

$$\partial_t f + v\partial_x f - E\partial_v f = 0, \tag{2.1}$$

$$\partial_x^2 \phi = \int_{-\infty}^{\infty} f \,\mathrm{d}v - 1, \tag{2.2}$$

where the space and time x and t, the electron velocity v, the electron distribution function $f(x, v, t)$, the electric field $E(x, t) = -\partial_x \phi$ and the corresponding electrostatic potential ϕ have been normalized by the Debye length $\lambda_D = \sqrt{\epsilon_0 k_B T/n_0 e^2}$, the inverse plasma frequency $\omega_p^{-1} = \sqrt{m\epsilon_0/n_0 e^2}$, the electron thermal speed $v_T = \sqrt{k_B T/m}$, $k_B T/e\lambda_D$ and $k_B T/e$, respectively. Here $-e$, m, T, n_0, ϵ_0 and k_B are the electron charge, mass, temperature, background density, the vacuum permittivity and Boltzmann constant, respectively. The ions form a uniform neutralizing background.

The evolution of the electron distribution function is followed by numerically solving the Vlasov equation using the standard split method of Cheng & Knorr (1976). Here, advances in the physical and velocity spaces are considered alternately in consecutive time steps. For example, in the first half time step $0 < t < \Delta t/2$ one advances in the physical space by solving $\partial_t f + v\partial_x f = 0$. In the next time step $\Delta t/2 < t < 3\Delta t/2$, one advances the velocity space with $\partial_t f - E\partial_v f = 0$. In the following half time step $3\Delta t/2 < t < 2\Delta t$, one again advances the physical space evolution $\partial_t f + v\partial_x f = 0$. All equations are solved using the Lax–Wendroff method. For the electric field, the centred-difference form of the Poisson equation is solved in each step using the Thomas algorithm together with Simpson integration. The periodic boundary conditions $f(x, v, t) = f(x + L, v, t)$ and $\phi(x, t) = \phi(x + L, t)$, where L is the width of simulated region, are used. For the calculations, the electron distribution satisfies $f(x, v, t) = 0$ for $|v| > v_m$, where v_m is a cutoff velocity satisfying $1 < v_m \ll c/v_T$, and c is the speed of light. The number of spatial grid points is N, and the number of velocity grid points is M. The time step $\mathrm{d}t$ satisfies the Courant–Friedrichs–Lewy condition. The numerical code is second-order accurate in time, space, and velocity, and can follow the electron velocity distribution accurately. The parameters $\mathrm{d}t$, v_m, N and M are selected according to the required accuracy, so that they can be different for different parameter regimes. There is no externally supplied initial perturbation of any of the physical variables. That is, the initial perturbations are from the very small but necessarily finite numerical noise. The code has been benchmarked against existing analytical and numerical results on linear and nonlinear Landau damping (Hou, Ma & Yu 2011*b*), as well as high-order plasma wave echoes (Hou, Ma & Yu 2011*a*).

3. Effect of the beam velocity

In a plasma with two counter-streaming electron components, one can expect unstable electrostatic electron oscillations (Hasegawa 1968, 1971; Clemmow &

https://doi.org/10.1017/S0022377815001087 Published online by Cambridge University Press

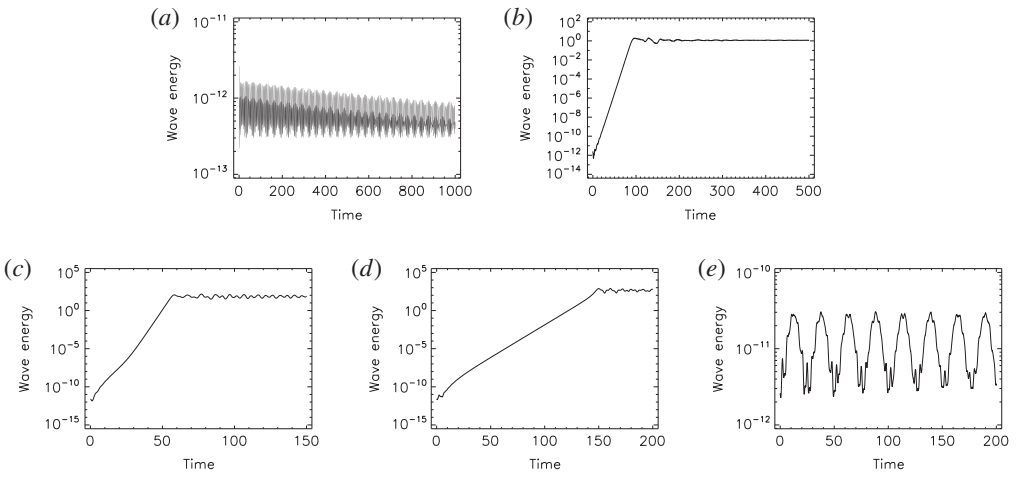


FIGURE 1. Evolution of the total wave energy for (*a*) $v_0 = 1$, $v_m = 11$, $\mathrm{d}t = 0.001$, (*b*) $v_0 = 2$, $v_m = 11$, $\mathrm{d}t = 0.001$, (*c*) $v_0 = 5$, $v_m = 16$, $\mathrm{d}t = 0.0005$, (*d*) $v_0 = 10$, $v_m = 23$, $\mathrm{d}t = 0.0005$, and (*e*) $v_0 = 11$, $v_m = 24$, $\mathrm{d}t = 0.0005$. Here we have assumed $L = 20\pi$, $N = 1024$, and $M = 3000$. There is no growth in (*a*) because the two peaks of the distribution function are too close (i.e. the region with unfavourable gradient is too small Clemmow & Dougherty 1969).

Dougherty 1969). To avoid the great variety of possible cases (Clemmow & Dougherty 1969), we shall restrict ourselves to considering the evolution of two counter-streaming electron plasmas given by the bi-Maxwellian equilibrium distribution function $f_0(v) = C(2\pi)^{-1/2} \exp[-(v - v_0)^2/2] + (1 - C)(2\pi)^{-1/2} \exp[-(v + v_0)^2/2]$, where C and $1 - C$ are the relative concentration of the two plasmas.

Figure 1 shows the evolution of the total wave electric field energy $\varepsilon_E = \int_0^L (E^2/2)\,\mathrm{d}x$ for $C = 0.5$ (i.e. two identical counter-streaming plasmas) and different values of v_0. As mentioned, for efficient and accurate numerical computation, appropriate values for v_m and $\mathrm{d}t$ are chosen for each case. Figure 1(*a*) for $v_0 = 1$ (i.e. in the marginally stable regime) shows that very small-amplitude transient plasma oscillations are initially excited by the noise, which depends on the space–time numerical accuracy, and the wave energy ε_E gradually damps. Figure 1(*b*) for $v_0 = 2$ (in the unstable regime) shows that after a short very low level ($\sim 10^{-12}$) transient stage, ε_E grows exponentially at a linear growth rate and eventually saturates at a high level ($\sim 10^{0}$) due to trapping of resonant electrons in the enhanced (nonlinear) wave field. Thereafter it oscillates at the effective bounce frequency of the trapped electrons. Figure 1(*c*) for $v_0 = 5$ and figure 1(*d*) for $v_0 = 10$ are similar to figure 1(*b*), except that here the linear growth stage consists of at least two different rates. As expected, the saturation level depends on the streaming velocity. Finally, figure 1(*e*) for $v_0 = 11$ shows that ε_E continues to fluctuate at a very low ($\sim 10^{-11}$) level.

The numerical results can be understood in terms of wave–particle interaction. When v_0 is very small, the unfavourable gradient $\partial_v f_0(v)$ and the separation of the two peaks in the electron distribution function are small and close to $v = 0$ (figure 2*a*). Plasma oscillations with such small phase velocities ω_p/k are of very short wavelengths, so that, in spite of the double-humped distribution function, instability does not occur (Clemmow & Dougherty 1969) (in the numerical calculation the short-wavelength modes are in fact precluded because of the finite grid size). As a

https://doi.org/10.1017/S0022377815001087 Published online by Cambridge University Press

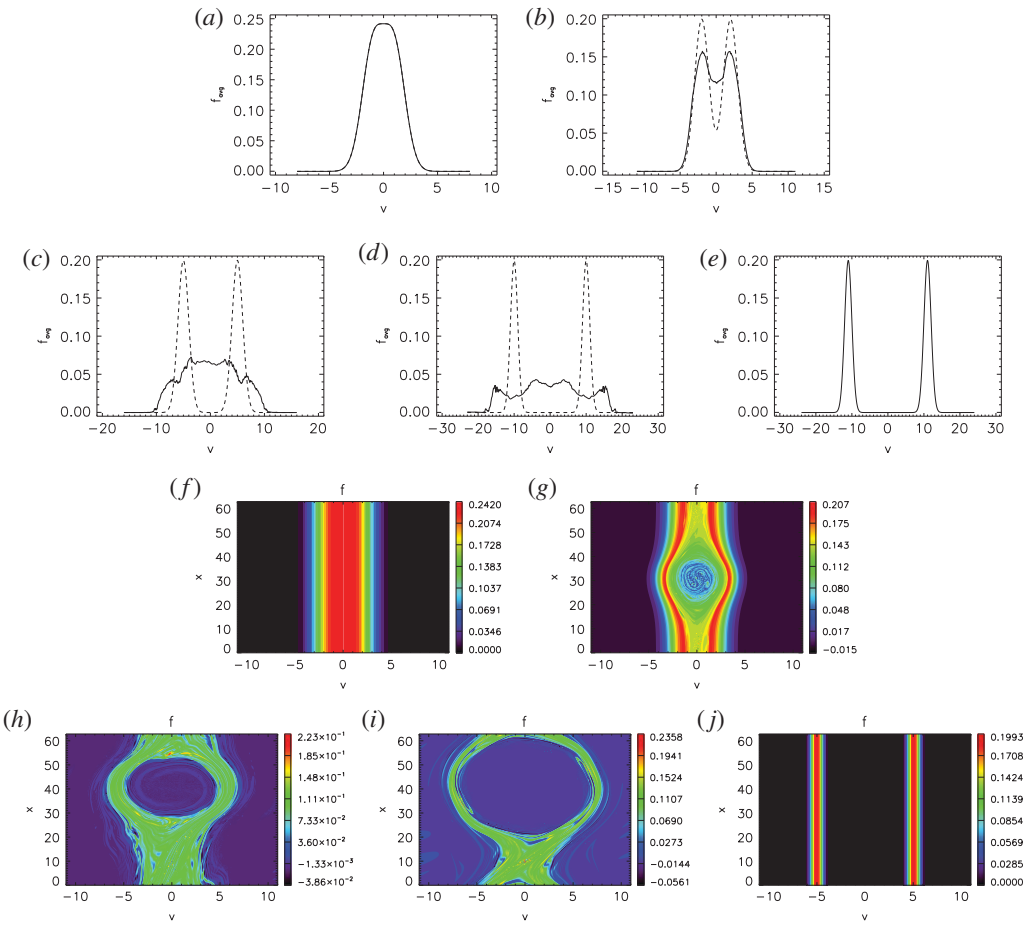


FIGURE 2. The space-averaged electron distribution function f_{avg} (*a–e*) and the corresponding phase space v, x (*f–j*) for, respectively, $v_0 = 1$, 2, 5, 10, and 11 at $t = 1000$, 500, 140, 200 and 200. Here, $f_{avg} = L^{-1}\int_0^L f(x, v)\,\mathrm{d}x$ is the velocity distribution function averaged over x. The dotted line is for the initial distribution $f_0(v) = (8\pi)^{-1/2}\{\exp[-(v - v_0)^2/2] + \exp[-(v + v_0)^2/2]\}$.

result, the total oscillation energy from the excited plasma oscillations and transients is damped because of numerical dissipation. There is thus little difference between the initial and final distribution functions, as shown in figure 2(*a*). There are also no trapped particles, as can be seen in figure 2(*f*). As v_0 increases, the two peaks of f_0 move apart, and the region as well as the magnitude of unfavourable gradient increase. Plasma waves with phase velocities in these regions suffer inverse Landau damping and instability appears. Figure 1(*b–d*) shows that the wave energy initially grows monotonically and eventually saturates, then it oscillates at a certain level. The initial growth in the wave energy is from the electron kinetic energy. Figure 2(*b–d*) shows that as the energy of the electrons is transferred to the waves, the velocity space distribution of the electrons becomes flattened. As the amplitude of the electric field of the growing waves increases, the electrons in phase with the wave can became trapped. As can be seen in figure 2(*g–i*), in this saturation stage the acceleration

https://doi.org/10.1017/S0022377815001087 Published online by Cambridge University Press

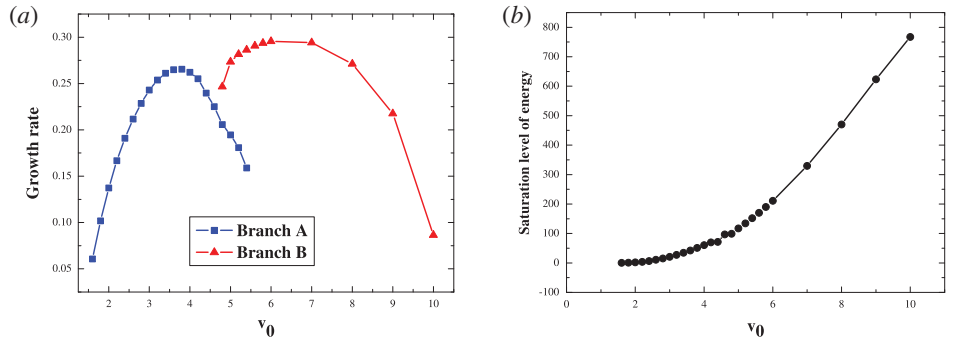


FIGURE 3. (*a*) The growth rate versus beam velocity v_0 and (*b*) the saturation level of energy versus beam velocity v_0 as obtained from the simulated wave energy ε_E. The two branches of the growth rate are due to the non-uniform growth behaviour of the latter, such as in figure 1(*c*,*d*).

and deceleration of the particles trapped in the wave potential wells lead to the oscillations in the wave energy. However, as can be seen in figure 1(*e*) for $v_0 = 11$, the instability disappears when v_0 becomes too large. Accordingly, there is little difference between the initial and final distribution functions in figure 2(*e*), and there are no trapped particles in figure 2(*j*). This is because the instability condition is no longer satisfied, and there are too few electrons in the region of the distribution function with unfavourable gradient, as shall be discussed in more detail below.

Thus, the evolution of the instability without an externally supplied initial perturbation can be separated into three temporal stages, namely the very small transient stage, the instability growth stage, and the saturation stage. In the small transient stage, the initial disturbance is from the numerical noise (and the magnitude is thus dependent on the numerical accuracy). In the next stage the wave electric field grows exponentially since the resonant electrons with velocity larger than the wave phase velocity lose their energy to the waves, resulting in flattening of the affected region of the distribution function. The saturation stage sets in when a sufficient number of resonant electrons become trapped by the enhanced wave electric field and oscillate between the potential walls. Circulation of the trapped electrons in the electron phase space forms vortex-like structures where energy exchange between the wave and the electrons occurs, resulting in the oscillation of wave energy.

Figure 1(*c*,*d*) for the evolution of the wave energy ε_E indicates that in the growth stage there can be overlapping of different linear (on the log scale) growth rates. In figure 3(*a*) we show that the total growth rate as a function of v_0 can indeed be decomposed into two regimes of v_0. In both regimes the growth rates first increase with v_0 and then decrease, but the corresponding v_0 regimes are very different. Figure 3(*b*) shows that the saturation level of the wave energy increases with v_0. This is to be expected since in both regimes saturation of the growth is due to electron trapping in the enhanced wave fields. As shall be discussed in more detail in the next section, this behaviour can be attributed to the growth of the different spatial harmonics of the excited waves.

4. Effect of different harmonics

The generation of harmonics during the evolution of beam–plasma or beam–beam instability was pointed out by Yoon (2000, 2005*a*,*b*). In order to see exactly what

https://doi.org/10.1017/S0022377815001087 Published online by Cambridge University Press

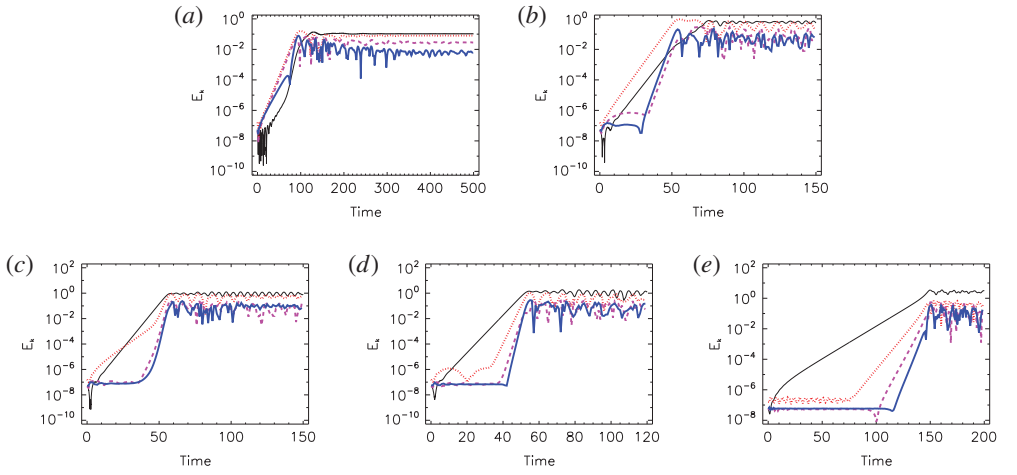


FIGURE 4. Evolution of the harmonics of the wave electric field for (*a*) $v_0 = 2$, $v_m = 11$, $\mathrm{d}t = 0.001$, (*b*) $v_0 = 4$, $v_m = 13$, $\mathrm{d}t = 0.0005$, (*c*) $v_0 = 5$, $v_m = 16$, $\mathrm{d}t = 0.0005$, (*d*) $v_0 = 6$, $v_m = 18$, $\mathrm{d}t = 0.0005$, and (*e*) $v_0 = 10$, $v_m = 23$, $\mathrm{d}t = 0.0005$. The black solid, red dotted, magenta dashed, and blue dash-dot-dot lines are for the first to the fourth harmonics, respectively. The parameters are $L = 20\pi$, $N = 1024$, $M = 3000$, and the time step is varied according to the resolution needed.

caused the non-uniform growth of the wave energy for different v_0 values, we have also carried out fast Fourier transform (FFT) of the wave electric field. Figure 4(*a–e*) shows how the first four harmonics of the wave electric field (i.e. E_k, $k = 1, \ldots, 4$, note the log scale in the figures) are excited and how each grows to saturation, followed by the trapping oscillations. It can be seen that the harmonics and their growth are not necessarily in sequence. When v_0 is small, in the initial growth stage the higher harmonics can dominate over the fundamental one and their regimes of dominance as well as times of saturation depend strongly but irregularly on v_0. The non-uniform growth of the total wave energy in the initial stage found in figure 1(*c*) can thus be attributed to this growth behaviour of the harmonics. For example, figure 4(*a*,*b*) shows that the second harmonic is dominant in the growth stage but the first harmonic becomes dominant in the saturation stage, and their saturation times are quite different. However, when v_0 is relatively large (figure 4*d*,*e*), the first harmonic is dominant and the higher harmonics are in sequence. The higher harmonics grow at larger rates and saturate at lower levels, which is qualitatively consistent with the result of Yoon (2005*b*). Among a large number of cases simulated, we found in general that the initial growth rate of the wave energy remains constant if and only if a single harmonic turns out to be dominant in the entire growth process, which is consistent with the linear instability theory. Figure 4(*c*) shows that when two or more harmonics compete, the growth stage of the total wave energy becomes non-uniform in time, as can be expected. The contributions of the different harmonics are also irregular, since they depend on the background and initial conditions as well as the evolution (recall that in the simulation phase space vortices are formed even when the wave amplitude is still very small). For example, we found that in figure 3(*a*) the second harmonic contributes more to branch A and the first harmonic more to branch B.

https://doi.org/10.1017/S0022377815001087 Published online by Cambridge University Press

5. Existence condition of instability

We have shown, by numerically solving the governing equations, that in the evolution of the bi-Maxwellian distribution, beam-type instabilities can take place. Here we consider in more detail the corresponding linear instabilities in terms of eigenmode analysis (Clemmow & Dougherty 1969).

The general dispersion relation for electrostatic waves in an electron plasma is $D(k, \omega) = 0$, where k is the wave vector, $\omega = \omega_r + \mathrm{i}\gamma$ is the sum of the wave frequency and growth/damping rate, and (Clemmow & Dougherty 1969)

$$D(k, \omega) = 1 - \frac{e^2}{\epsilon_0 m k^2} \int_{-\infty}^{\infty} \frac{\mathrm{d}_v f_0(v)}{v - \omega/k}\, \mathrm{d}v. \tag{5.1}$$

For $\gamma \ll \omega_r$, γ is given by

$$\gamma = -(\pi\omega_p/2k)\mathrm{d}_v f_0(v)|_{v=\omega_r/k}(\omega_r/k - \mathrm{d}_k\omega_r), \tag{5.2}$$

so that a mode of frequency ω_r can grow if $\mathrm{d}_v f_0(v) > 0$, corresponding to inverse Landau damping. The latter has been attributed to resonant energy exchange with the wave and the electrons with velocities near the wave phase velocity, or $v \sim \omega_r/k$.

The existence condition and growth rate of the beam instability can be estimated from the cold plasma limit (replacing the Gaussian functions in f_0 by delta functions) since thermal effects do not contribute significantly to the instability (Clemmow & Dougherty 1969). The linear dispersion relation for two counter-propagating electron beams is then (Clemmow & Dougherty 1969; Chen 1984; Boyd & Sanderson 2003)

$$\frac{\omega_{pa}^2}{(\omega - kv_0)^2} + \frac{\omega_{pb}^2}{(\omega + kv_0)^2} = 1, \tag{5.3}$$

where $\omega_{pa} = \sqrt{C}\omega_p$ and $\omega_{pa} = \sqrt{1 - C}\omega_p$ are the plasma frequencies of the two beams.

The purely growing beam instability appears for $0 < k < k_{cr}$, where

$$k_{cr} = [(C^{1/3} + (1 - C)^{1/3})^{3/2}]\omega_p/2v_0. \tag{5.4}$$

Physically, this instability is caused by a phase mismatch (due to electron bunching) in the restoring force of the beam-driven electron oscillations, which are thereby destroyed. For the case $C = 0.5$, the beam mode can be written

$$\omega^2 = k^2v_0^2 + \omega_p^2/2 \pm \omega_p/\sqrt{2}\left[\omega_p^2/2 + 4k^2v_0^2\right]^{1/2} \tag{5.5}$$

and the corresponding critical wave vector is $k_{cr} = \omega_p/v_0$. In the unstable regime, we can obtain, by setting $\mathrm{d}_k\omega = 0$, the maximum growth rate $\omega_p/2\sqrt{2}$, occurring for $k = \sqrt{3}\omega_p/2\sqrt{2}v_0$. For the simulation where $L = 20\pi$ and $M = 3000$, we get $1/10 < k < 300$. That is, when $v_0 = 6$ (first harmonic dominates, see figure 4*d*)), the growth rate is maximum (figure 3*a*), and correspondingly $k \sim 1/10$.

In the simulations the wavelength of the noise-excited mode is necessarily in the range $2\pi/L < k < 2M\pi/L$, where M is an integer. The existence condition for instability is then $k_{cr} \geqslant k_{min}$, where k_{min} is the minimum wave vector allowed in the simulation, that is, $v_0 \leqslant v_{cr}$, where the critical velocity is $v_{cr} = (C^{1/3} + (1 - C)^{1/3})^{3/2}\omega_p L/4\pi$, or $L \geqslant L_{cr}$, where the critical system size is $L_{cr} = 4\pi(C^{1/3} + (1 - C)^{1/3})^{-3/2}v_0/\omega_p$.

https://doi.org/10.1017/S0022377815001087 Published online by Cambridge University Press

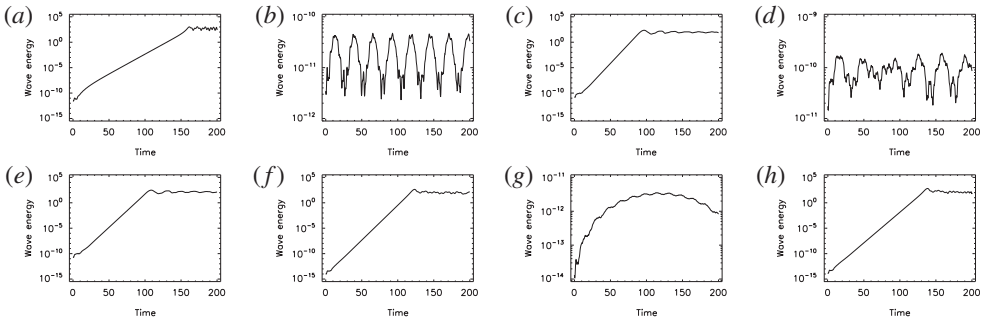


FIGURE 5. Evolution of the wave energy for (*a*) $v_0 = 11$ and $L = 22\pi$, (*b*) $v_0 = 12$ and $L = 22\pi$, (*c*) $v_0 = 8$ and $L = 20\pi$, (*d*) $v_0 = 9$ and $L = 20\pi$, (*e*) $v_0 = 9$ and $L = 22\pi$, (*f*) $v_0 = 9$ and $L = 20\pi$, (*g*) $v_0 = 10$ and $L = 20\pi$, and (*h*) $v_0 = 10$ and $L = 22\pi$.

In order to see if these cold-plasma results are applicable to the initial (linear) stage of the instabilities, we have carried out simulations of the instability for several parameter regimes. Figure 1(*e*) is for $L = 20\pi$ and $v_0 = 11$. Since $v_{cr} = 10$, there is no instability, as predicted. Also as expected, figure 5(*a*,*b*) shows that with $L = 22\pi$ instability occurs for $v_0 = 11$ but not for $v_0 = 12$ since here $v_{cr} = 11$. Furthermore, for $C = 0.1$ and $L = 20\pi$ we have $v_{cr} = 8.547$, and figure 5(*c*,*d*) shows that instability indeed occurs for $v_0 = 8$ but not for $v_0 = 9$. Figure 5(*e*) for $L = 22\pi$ and $v_0 = 9$ shows that instability occurs since here $v_{cr} = 9.4$. Moreover, for $C = 0.2$ and $L = 20\pi$, the critical velocity is $v_{cr} = 9.3$ and figure 5(*f*,*g*) verifies that instability does occur for $v_0 = 9$ but not for $v_0 = 10$. Finally, figure 5(*h*) for $L = 22\pi$ and $v_0 = 10$ shows that instability occurs as expected, since here $v_{cr} = 10.24$. Thus, the simulation results are quite consistent with those from the theory.

6. Discussion

In this work, electrostatic two-stream instabilities have been considered in more detail by numerically solving the Vlasov–Poisson system. It is found that the beam instability can have different growth rates during the initial stage because of the coexisting harmonics of the beam mode.

Like the Penrose criteria (Penrose 1960), our simulation does not explicitly distinguish the modes involved. Our results on the linear stage (when the growth is exponential) of the instability are also consistent with the Penrose criteria, e.g. a two-stream plasma is linearly unstable if the background distribution has a minimum (always satisfied for the bi-Maxwellian distribution), and

$$\int_{-\infty}^{\infty} \frac{f_0(v) - f_0(\omega/k)}{(v - \omega/k)^2}\,\mathrm{d}v > 0, \tag{6.1}$$

so that instability does not occur if the electron temperature is too high with respect to the relative streaming velocity $2v_0$, or $2v_0 \geqslant 1$ for $C = 0.5$ (Clemmow & Dougherty 1969; Boyd & Sanderson 2003) in our simulations. As two-stream instabilities provide an efficient way for transferring kinetic energy of the plasma particles to the wave energy, the results here should also be useful for problems in fusion plasmas (Wu 2006, 2008; Wu, Jiang & Wang 2011) and space plasmas. On the other hand, we have not included the higher-dimensional effects that are ubiquitous in realistic plasmas

https://doi.org/10.1017/S0022377815001087 Published online by Cambridge University Press

because of the existence of external electric and magnetic fields, plasma boundaries and interfaces, etc. To include higher-dimensional effects, more elaborate and efficient Vlasov codes will be needed (Eliasson 2010). It may also be of interest to point out that the two-stream instability can also be important in solid-state, cosmic and quantum plasmas (Kohn 1999; Eliasson & Shukla 2010; Scholl *et al.* 2013; Uzdensky & Rightley 2014; Haas & Eliasson 2015).

Acknowledgements

The authors would like to thank other members of the FDS team for the support, as well as J. Q. Jiang, M. H. Wang and M. Y. Ni for useful discussions. This work has been supported by the National Natural Science Foundation of China (11205194, 11374262), the Fundamental Research Funds for Central Universities, and the State Key Laboratory of High Field Laser Physics at SIOM.

REFERENCES

BOYD, T. J. M. & SANDERSON, J. J. 2003 *The Physics of Plasmas*. Cambridge University Press.

CHEN, F. F. 1984 *Introduction to Plasma Physics*. Plenum.

CHENG, C. Z. & KNORR, G. 1976 The integration of the Vlasov equation in configuration space. *J. Comput. Phys.* **22**, 330–351.

CLEMMOW, P. C. & DOUGHERTY, J. P. 1969 *Electrodynamics of Particles and Plasmas*. Addison-Wesley.

DALDORFF, L. K. S., PECSELI, H. L., TRULSEN, J. K., ULRIKSEN, M. I., ELIASSON, B. & STENFLO, L. 2011 Nonlinear beam generated plasma waves as a source for enhanced plasma and ion acoustic lines. *Phys. Plasmas* **18**, 052107.

DENEEF, C. P., MALMBERG, J. H. & O'NEIL, T. M. 1973 Launched waves on a beam-plasma system. *Phys. Rev. Lett.* **30**, 1032–1035.

DIECKMANN, M. E., ELIASSON, B., SHUKLA, P. K., SIRCOMBE, N. J. & DENDY, R. O. 2006 Two-stream instability in collisionless shocks and foreshock. *Plasma Phys. Control. Fusion* **48**, B303–B311.

EL-LABANY, S. K. & ROWLANDS, G. 1986 The non-linear two-stream problem–a new approach. *Plasma Phys. Control. Fusion* **28**, 1549–1558.

ELIASSON, B. 2010 Numerical simulations of the Fourier-transformed Vlasov – Maxwell system in higher dimensions–theory and applications. *Transp. Theory Stat. Phys.* **39**, 387–465.

ELIASSON, B. & SHUKLA, P. K. 2010 Dispersion properties of electrostatic oscillations in quantum plasmas. *J. Plasma Phys.* **76**, 7–17.

FIJALKOW, E. & NOCERA, L. 2005 Superposition of phase-space hole streets in Vlasov plasmas. *J. Plasma Phys.* **71**, 401–410.

GENTLE, K. W. & HOHR, J. 1973 Phase-space evolution of a trapped electron beam. *Phys. Rev. Lett.* **30**, 75–77.

HAAS, F. & ELIASSON, B. 2015 A new two-stream instability mode in magnetized quantum plasma. *Phys. Scr.* **90**, 088005.

HARTMANN, D. A., DRISCOLL, C. F., O'NEIL, T. M. & SHAPIRO, V. D. 1995 Measurements of the weak warm beam instability. *Phys. Plasmas* **2**, 654–677.

HASEGAWA, A. 1968 Theory of longitudinal plasma instabilities. *Phys. Rev.* **169**, 204–214.

HASEGAWA, A. 1971 Plasma instabilities in the magnetosphere. *Rev. Geophys.* **9**, 703–772.

HOU, Y. W., MA, Z. W. & YU, M. Y. 2011*a* The plasma wave echo revisited. *Phys. Plasmas* **18**, 012108.

HOU, Y. W., MA, Z. W. & YU, M. Y. 2011*b* Trapped particle effects in long-time nonlinear Landau damping. *Phys. Plasmas* **18**, 082101.

INFELD, E. & SKORUPSKI, A. 1970 The two-stream instability and its classification into absolute and convective for hot plasmas. *J. Plasma Phys.* **4**, 607–615.

https://doi.org/10.1017/S0022377815001087 Published online by Cambridge University Press

KOHN, W. 1999 Nobel lecture: electronic structure of matter–wave functions and density functionals. *Rev. Mod. Phys.* **71**, 1253–1266.

LACINA, J., KRLIN, L. & KORBEL, S. 1976 Effect of beam density and of higher harmonics on beam–plasma interaction. *Plasma Phys.* **18**, 471–483.

MOREY, I. J. & BOSWELL, R. W. 1989 Evolution of bounded beam–plasma interactions in a one-dimensional particle simulation. *Phys. Fluids* B **1**, 1502–1510.

MORSE, R. L. & NIELSON, C. W. 1969 One-, two-, and three-dimensional numerical simulation of two-beam plasmas. *Phys. Rev. Lett.* **23**, 1087–1090.

NG, C. S., BHATTACHARJEE, A. & SKIFF, F. 2004 Complete spectrum of kinetic eigenmodes for plasma oscillations in a weakly collisional plasma. *Phys. Rev. Lett.* **92**, 065002.

PENROSE, O. 1960 Electrostatic instabilities of a uniform non-Maxwellian plasma. *Phys. Fluids* **3**, 258–265.

ROBERTS, K. V. & BERK, H. L. 1967 Nonlinear evolution of a two-stream instability. *Phys. Rev. Lett.* **19**, 297–300.

ROSTOMIAN, E. V. 1994 The dynamics of superdense electron beam instability in plasma. *Plasma Phys. Control. Fusion* **36**, 1737–1742.

SCHAMEL, H. 1982 Stability of electron vortex structures in phase space. *Phys. Rev. Lett.* **48**, 481–483.

SCHOLL, J. A., GARCIA-ETXARRI, A., KOH, A. L. & DIONNE, J. A. 2013 Observation of quantum tunneling between two plasmonic nanoparticles. *Nano Lett.* **13**, 564–569.

UZDENSKY, D. A. & RIGHTLEY, S. 2014 Plasma physics of extreme astrophysical environments. *Rep. Prog. Phys.* **77**, 036902.

VAN-WAKEREN, J. H. A. & HOPMAN, H. J. 1975 Thermalization of a beam by beam-plasma interaction. *J. Plasma Phys.* **13**, 349–360.

VOLOKITIN, A. & KRAFFT, C. 2012 Velocity diffusion in plasma waves excited by electron beams. *Plasma Phys. Control. Fusion* **54**, 085002.

WHELAN, D. A. & STENZEL, R. L. 1983 Nonlinear energy flow in a beam-plasma system. *Phys. Rev. Lett.* **50**, 1133–1136.

WU, Y. 2006 Conceptual design activities of FDS series fusion power plants in China. *Fusion Engng Des.* **81**, 2713–2718.

WU, Y. 2008 Conceptual design of the China fusion power plant FDS-II. *Fusion Engng Des.* **83**, 1683–1689.

WU, Y., JIANG, J., WANG, M., JIN, M. & FDS TEAM 2011 A fusion-driven subcritical system concept based on viable technologies. *Nucl. Fusion* **51**, 103036.

YOON, P. H. 2000 Generalized weak turbulence theory. *Phys. Plasmas* **7**, 4858–4871.

YOON, P. H. 2005*a* Effects of spontaneous fluctuations on the generalized weak turbulence theory. *Phys. Plasmas* **12**, 042306.

YOON, P. H. 2005*b* Progress in the kinetic theory of electrostatic harmonics of plasma waves. *Phys. Plasmas* **12**, 052313.

ZHENG, C. Y., LIU, Z. J., ZHANG, A. Q., ZHU, S. P. & HE, X. T. 2006 Simulation of electron beam instabilities in collisionless plasmas. *J. Plasma Phys.* **72**, 249–258.

https://doi.org/10.1017/S0022377815001087 Published online by Cambridge University Press